Criteria of backscattering in chiral one-way photonic crystals

Pi-Ju Cheng[a] and Shu-Wei Chang[a,b*]

[a]Research Center for Applied Sciences, Academia Sinica, 11529, Taipei, Taiwan.
[b]Department of Photonics, National Chiao-Tung University, 30010, Hsinchu, Taiwan.

*swchang@sinica.edu.tw

ABSTRACT

Optical isolators are important devices in photonic circuits. To reduce the unwanted reflection in a robust manner, several setups have been realized using nonreciprocal schemes. In this study, we show that the propagating modes in a strongly-guided chiral photonic crystal (no breaking of the reciprocity) are not backscattering-immune even though they are indeed insensitive to many types of scatters. Without the protection from the nonreciprocity, the backscattering occurs under certain circumstances. We present a perturbative method to calculate the backscattering of chiral photonic crystals in the presence of chiral/achiral scatters. The model is, essentially, a simplified analogy to the first–order Born approximation. Under reasonable assumptions based on the behaviors of chiral photonic modes, we obtained the expression of reflection coefficients which provides criteria for the prominent backscattering in such chiral structures. Numerical examinations using the finite-element method were also performed and the results agree well with the theoretical prediction. From both our theory and numerical calculations, we find that the amount of backscattering critically depends on the symmetry of scatter cross sections. Strong reflection takes place when the azimuthal Fourier components of scatter cross sections have an order l of 2. Chiral scatters without these Fourier components would not efficiently reflect the chiral photonic modes. In addition, for these chiral propagating modes, disturbances at the most significant parts of field profiles do not necessarily result in the most effective backscattering. The observation also reveals what types of scatters or defects should be avoided in one-way applications of chiral structures in order to minimize the backscattering.

Keywords: Photonic crystal, Backscattering, Chiral optics

1. INTRODUCTION

Reducing unwanted reflections and backscattering during wave transmissions and propagations is pivotal in photonic integrated systems. It lowers potential channel noises and interferences and therefore necessitates the photonic device such as isolators[1]. Such devices only transmit the optical power unidirectionally but block the energy flow in the reverse direction. To implement this functionality in a robust manner, various nonreciprocal setups are proposed. In electronics, the one-way phenomenon is present in the edge states of quantum Hall effect due to a high magnetic field that breaks the time-reversal symmetry[2-4]. Analogously, in photonics, unidirectional edge modes can be also achieved using photonic crystals (PhCs) with static magneto-optical effects[5-7] or dynamic phase modulations[8-10]. Despite various nonreciprocal schemes targeting at one-way behaviors of waves, their compatibilities with photonic systems nowadays still require some key progress. Since most of the conventional linear optical devices are reciprocal, enormous efforts have to be devoted to the integration of nonreciprocal (magnetic) materials or complicated time-variant controls to photonic structures. These inconveniences motivate the development of reciprocal schemes which isolate energy flows in opposite directions. For example, asymmetric two-way transmissions may be achieved through designed gratings[11-13]. In wave-guiding structures, reciprocal modes that are backscattering-immune to a variety of scatters are preferred so that energy flows are not easily reversed. This, however, does not mean only unidirectional modes are supported. In fact, in reciprocal environments, counter-propagating modes always exist simultaneously, namely, a reciprocal photonic system is bidirectional[14].

Two elements are essential to the immunity of modes (states) to backscattering in reciprocal (time-reversible) systems. If (1) the counter-propagating modes (states) are firmly associated with some orthogonal degrees of freedom (DOFs), and (2) elastic scatters do not mix these DOFs, the backscattering is suppressed. Such characteristics can be

Physics and Simulation of Optoelectronic Devices XXIV, edited by
Bernd Witzigmann, Marek Osiński, Yasuhiko Arakawa, Proc. of SPIE Vol. 9742,
97420N · © 2016 SPIE · CCC code: 0277-786X/16/$18 · doi: 10.1117/12.2210760

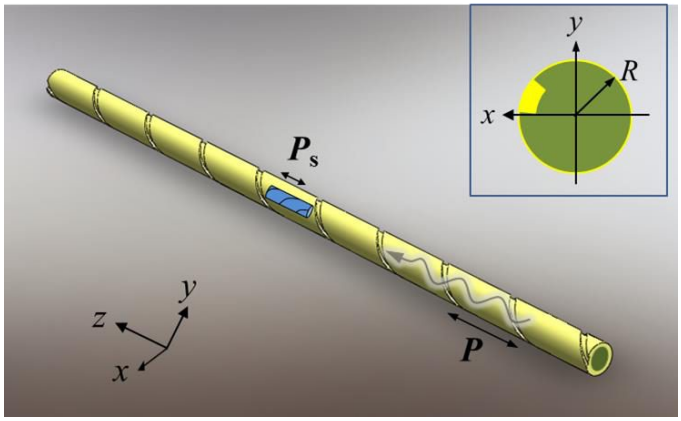

Figure 1. The schematic diagram of the one-way chiral PhC covered by PECs. A chiral scatter is inserted into the wave-guiding structure. The top inset shows a generic cross section inside the PhC.

found in the edge modes (states) of photonic (electronic) topological insulators[15-17]. In fact, these prerequisites on one-way propagations are also present in circularly-polarized (CP) guided modes of one-dimensional (1D) chiral PhCs or waveguides (WGs)[18-20]. In this case, the key DOFs are the two circular polarizations rotating in opposite orientations. Absence of backscattering from simple scatters has also been demonstrated experimentally in 1D chiral PhCs[20].

While the aforementioned condition (2) may hold for a broad range of scatters, there are always exceptions. The breakdown of this condition indicates the onset of backscattering. This point motivates us to examine the robustness of reciprocal chiral guided modes against the backscattering. Here, we look into the dependencies of backscattering on geometries of different scatters in a 1D chiral PhC covered by perfect electric conductors (PECs) at microwave frequencies. We use the first-order Born approximation and coupled-mode theory to develop the criteria of prominent scattering in the chiral structure. The outcomes indicate that the amount of backscattering closely depends on the cross-sectional symmetry of scatters. In addition, even if the scatter is placed at positions corresponding to the most intense parts of mode profiles, the backscattering there is not necessarily the most prominent. The behavior is contrary to that of typical backscattering in typical WGs. Our studies also point out what types of scatters or defects should be avoided in one-way applications of chiral structures so that the backscattering could be minimized.

2. ONE-WAY CHIRAL PHOTONIC CRYSTAL

The schematic diagram of the 1D chiral PhC in this study is shown in Fig. 1. This chiral structure is generalized from a circular PEC WG with a radius R = 1 cm, and its center is coincident with the z axis. The interior of the PhC is filled with air and has a relative permittivity of unity. A generic cross section of the PhC is shown in the top inset of Fig. 1. A PEC bump in the form of a truncated sector is present at the circular rim. The chiral PhC is a right-handed (RH) structure and has a pitch P. Since its cross section does not have any rotational symmetry, the pitch P is also the period of this PhC.

In absence of the bump, eigenmodes of the circular PEC WG are analytically solvable. They can be divided into transverse-electric (TE) modes TE_{mn} and transverse-magnetic (TM) modes TM_{mn}, where m and n are the azimuthal and radial mode numbers, respectively. Hereafter, we adopt the representation $\exp(im\phi)/\sqrt{2\pi}$ for azimuthal parts of various cylindrical field components. The fundamental modes are two degenerate TE modes $TE_{\pm 1,1}$. These two modes are of interest since their polarization patterns are close to circular polarizations and can properly grasp features of the chirality. With optic conventions for waves propagating toward the direction of positive z axis, the $TE_{+1,1}$ and $TE_{-1,1}$ modes are similar to the left-handed circularly-polarized (LHCP) and right-handed circularly-polarized (RHCP) waves with polarizations $\hat{e}_+ = (\hat{x} + i\hat{y})/\sqrt{2}$ and $\hat{e}_- = \hat{e}_+^*$, respectively. On the other hand, upon reversing the propagation toward the direction of negative z axis, the LHCP and RHCP waves change their polarizations into $\hat{e}_-$ and $\hat{e}_+$, and they are therefore associated with $TE_{-1,1}$ and $TE_{+1,1}$ modes, respectively.

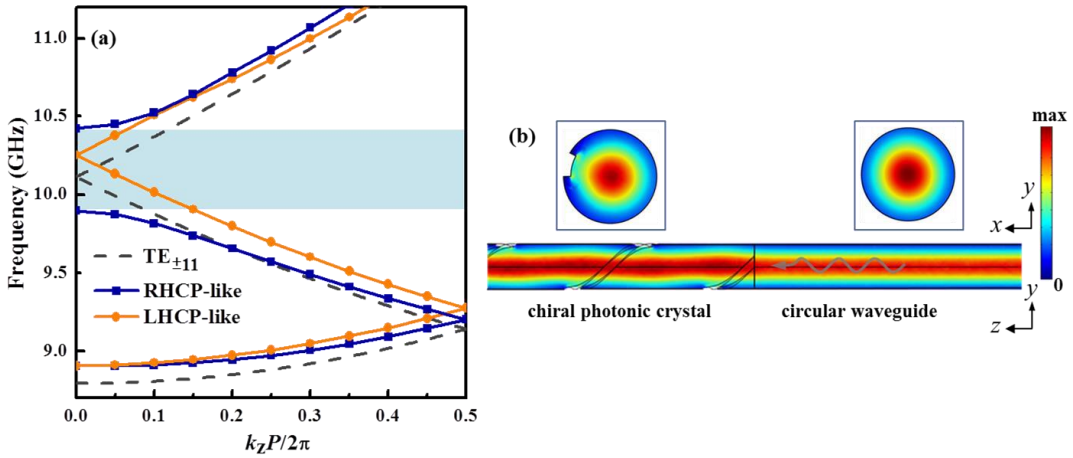

Figure 2. (a) Bandstructures of the 1D chiral PhC. The dispersion curves of the unperturbed TE modes are split into those of the LHCP-like and RHCP-like modes. The RHCP-like mode has a chiral band gap at the BZ center. (b) The incidence of a forward-propagating TE mode from the circular WG into chiral PhC. The cross-sectional distributions of square field magnitudes in the WG and PhC regions are shown at the top. Except for areas near the bump, the two field patterns appear similar.

The pitch P is set to 6 cm so that the chiral bandgap responsible for one-way propagations is opened between the cutoff frequencies of $TE_{\pm 1,1}$ and $TM_{0,1}$ modes. Figure 2(a) shows bandstructures of the chiral PhC around the frequency range of interest in the first Brillouin zone (BZ) for wave number k_z~0. The calculations are carried out with the eigenfrequency solver of commercial software COMSOL[21]. The dispersion curves of $TE_{\pm 1,1}$ modes are also shown in the scheme of reduced zones for comparisons. The chiral bump breaks the degeneracy of $TE_{\pm 1,1}$ modes and turn them into the LHCP-like and RHCP-like modes. While the dispersion curve of LHCP-like modes is only slightly shifted in frequencies as compared to that of $TE_{\pm 1,1}$ modes, an additional chiral bandgap from 9.90 to 10.42 GHz is developed on the counterpart of RHCP-like modes at the BZ center due to the RH chiral structure. As an examination of the similarity between the $TE_{\pm 1,1}$ and forward-propagating LHCP-like modes, we monitor the incidence of the $TE_{\pm 1,1}$ mode from the circular WG to the chiral PhC at a frequency of 10.16 GHz within the chiral bandgap. The cross-sectional view of the field pattern near the junction of the WG and PhC is illustrated in Fig. 2(b). Only minor reflections and field variations due to the discontinuity of the wave-guiding structure are observed. As shown at the top of Fig. 2(b), the cross-sectional distributions of field strengths in the WG and PhC regions are similar except for areas near the bump. This test confirms the resemblance between the $TE_{+1,1}$ mode of the circular WG and forward-propagating LHCP-like mode of the chiral PhC. Since no significant reflections are observed here, this incidence scheme will be utilized later to excite the forward-propagating LHCP-like mode.

In the frequency range of this chiral bandgap, only LHCP-like modes can propagate while RHCP-like ones behave like evanescent waves. Since the forward- and backward-propagating LHCP-like modes have distinct polarizations patterns similar to $\hat{e}_+$ and $\hat{e}_-$, respectively, the two waves would simply pass by those scatters which cannot mix polarizations and hence are not effectively reflected. We will focus on chiral scatters with a pitch P_s and cross sections of different rotational symmetries. As will be shown later, chiral scatters reflect the propagating modes effectively even though other types of scatters could also result in backscattering.

3. CRITERIA FOR PROMINENT BACKSCATTERING

In this section, we briefly describe the concepts in constructing the analytical model. In short, we use a perturbative scheme to investigate the backscattering in the chiral PhC. Details about the theoretical model of backscattering can be found in Ref. [22].

Instead of solving the full field inside the chiral PhC in the presence of scatters, the first-order Born approximation is utilized to turn this problem into an effective radiation counterpart. An effective source is present as a result of the coupling between the incident field and permittivity variation $\Delta\varepsilon_{r,s}(\mathbf{r},\omega)$ due to the scatter. The generalized reciprocity theorem is utilized to formulate the coupled mode theory for the scattered fields in the chiral PhC. The frequency range of the chiral bandgap is designed such that only the fundamental modes of the circular PEC WG are required to properly expand the scattered field. At this frequency in the middle of chiral bandgap, only the LHCP-like modes can propagate. Coupled mode formulae could be further simplified after some physical approximations. The reflection coefficient which is the ratio between the back-propagating amplitude and incident amplitude is derived to quantify the amount of backscattering.

The reflection coefficient $r(\omega)$ is affected by the interplay between $\Delta\varepsilon_{r,s}(\mathbf{r},\omega)$ and other two factors. Its functional dependence can be expressed as

$$r(\omega) \propto \int_{\Omega_s} d\mathbf{r}' \exp[2i(\phi' + qz')] \cdot \Delta\varepsilon_{r,s}(\mathbf{r}',\omega) \cdot \left\{ \left[\frac{J_1(k_t\boldsymbol{\rho}')}{k_t\boldsymbol{\rho}'} \right]^2 - [J_1'(k_t\boldsymbol{\rho}')]^2 \right\}, \tag{1}$$

where $q=2\pi/P$; $k_t \sim 1.84/R$; J_1 is Bessel function of the first-kind; and Ω_s is the scatter region. The first factor is the phase part $\exp[2i(\phi' + qz')]$, and the second one is related to the transverse fundamental TE mode profile. For the former, the cancelation of the phase part generally enhances the volume integral in Eq. (1) even though the effect is relatively minor for small scatters. In other words, the prominent backscattering would occur if $\Delta\varepsilon_{r,s}(\mathbf{r},\omega)$ can cancel the phase factor. To result in the strong backscattering, we expect an effective scatter to be a LH chiral structure with (1) a pitch P_s close to P and (2) a significant azimuthal Fourier component of $\Delta\varepsilon_{r,s}(\mathbf{r},\omega)$ at an order $l=-2$. Let us further write the permittivity variation $\Delta\varepsilon_{r,s}(\mathbf{r},\omega)$ of such a LH chiral scatter as

$$\Delta\varepsilon_{r,s}(\mathbf{r}',\omega) = U(\mathbf{r}') \sum_{l=-\infty}^{\infty} \Delta\varepsilon_{r,s}^{(l)}(\rho',\omega)\, e^{il(\phi' + q_s z')}. \tag{2}$$

where U denotes an indicator function which is unity in the scatter region Ω_s but zero elsewhere; and $q_s=2\pi/P_s$. From Eq. (2), if $\Delta\varepsilon_{r,s}(\mathbf{r},\omega)$ has the f-fold rotational symmetry along the z-axis, only the components with their order l that are multiples of f would exist. If f is larger than 2, the component with $l=-2$ vanishes. Therefore, the prominent backscattering is most likely to occurs for proper LH chiral scatters with two-fold rotationally symmetric or rotationally asymmetric cross sections ($f=1, 2$).

For the effect of the second factor, we may consider a small scatter Ω_s at radial position ρ_s with a narrow range $\Delta\rho_s$ in the radial direction. In this case, the reflection coefficient has an approximate radial dependency characterized by a function $g(\rho_s) = [J_1(k_t\rho_s)/k_t\rho_s]^2 - [J_1'(k_t\rho_s)]^2$, that is, we may rewrite Eq. (1) as

$$r(\omega) \sim \rho_s \Delta\rho_s g(\rho_s) \int_{\boldsymbol{\rho}_s - \Delta\boldsymbol{\rho}_s/2}^{\boldsymbol{\rho}_s + \Delta\boldsymbol{\rho}_s/2} d\boldsymbol{\rho}' \frac{\Delta\varepsilon_{r,s}(\mathbf{r}',\omega)}{\Delta\boldsymbol{\rho}_s} [\ldots], \tag{3}$$

where the radial integral is an average of $\Delta\varepsilon_{r,s}(\mathbf{r}',\omega)$ around $\rho'=\rho_s$; and […] represents details other than the radial integral. The behavior of $g(\rho_s)$ indicates that the prominent backscattering in the chiral PhC takes place as the scatter is near the rim of the structure, at which the modal intensity is low.

4. NUMERICAL RESULTS

With a LHCP-like incident mode of the circular PEC WG at 10.16 GHz, we solve the scattered field inside the chiral PhC using the three-dimensional finite-element method implemented in COMSOL. Both ends of the computation domain are set to perfectly matched layers to make the scattered field outgoing. The power reflectivity $|r(\omega)|^2$ is then obtained from the incident and total fields. Unless otherwise mentioned, there are 32 pitches of chiral structures at each side of scatters. We first consider fictitious chiral scatters with f-fold (f =2 to 4) rotationally symmetric cross sections, which are composed of $2f$ identical truncated sectors with permittivity variations alternating in signs [$\Delta\varepsilon_{r,s}(\mathbf{r},\omega) = \pm\Delta\varepsilon_{r,s}$]. For conveniences, we will simply call the scatters as f-fold LH/RH scatters. The radii R_s of these scatters will be varied, but for fair comparisons, their radial widths are adjusted accordingly so that their cross-sectional areas remain unaltered.

The cross-sectional geometry of the 2-fold LH scatters as the radius R_s increases is shown in Fig. 3(a) (arrow indicates the handedness). The cross-sectional areas are fixed at $0.3\pi R^2$. The side view of the scatter is shown in Fig. 3(b). The scatter pitches P_s and lengths of the scatters are both set to P. The reflectivities versus R_s at different permittivity variations $\Delta\varepsilon_{r,s}$ = 0.5, 0.6, and 0.7 are shown in Fig. 4. Although these variations are comparable to the background permittivity set as unity, the trends of reflectivities versus Rs qualitatively follow the function $|g(\rho_s)|^2$, indicating that the first-order Born approximation and coupled-mode theory work well in these cases. As R_s~$0.27R$, the scatter cross sections are filled circles and have the best overlap with the most intense portion of the LHCP-like mode. However, the corresponding power reflectivities are minimal. As R_s becomes large, the reflectivities significantly increase. This characteristic indicates that to avoid the prominent backscattering in this chiral PhC, the fluctuations and defects near the rim of the wave-guiding structure should be reduced. On the other hand, the 2-fold RH scatters only backscatter weakly, as shown in Fig. 4(b). They exhibit small power reflectivities that do not seem to have a consistent trend as R_s increases, partly due to the compromise between computational accuracies and dense meshes used in calculations. However, it is certain that the smallness of reflectivities originates from the inability of 2-fold RH scatters to compensate the phase factor in Eq. (1). Similar to the 2-fold RH scatter, the 3-fold and 4-fold LH scatters do not backscatter significantly because they only have the azimuthal Fourier components at $l \geq 3$ and hence cannot compensate the phase factor. The power reflectivities of these two scatters as a function R_s at different $\Delta\varepsilon_{r,s}$ are shown in Fig. 4(c) and (d), respectively.

In Fig. 5(a) and (b), we show the field distributions $|\mathbf{E}(\mathbf{r})|^2$ around the 2-fold LH and RH scatters with $R_s = 0.7R$ and $\Delta\varepsilon_{r,s}$ = 0.7 on the y-z plane. The RH scatter seems to backscatter little, as can be told from seemingly unaltered magnitudes of the propagating waves at its two sides. The field distributions near the 3-fold and 4-fold LH scatters with $R_s = 0.3R$ and $\Delta\varepsilon_{r,s}$ = 0.7 are depicted in Fig.5(c) and (d). There are significant local fields confined in the two scatters. However, the local fields mostly correspond to the evanescent modes in the chiral PhC. One can tell that the magnitudes of the propagating waves in the front and backsides of the two scatters remain nearly identical.

At last, we model the numerical reflection coefficient of a small scatter as a function of its position ρ_s from the center of the chiral PhC using the functional form of $g(\rho_s)$. As shown in the inset of Fig. 6, we consider a small copper block with a size of $0.3R \times 0.5R \times 0.5R$ and move it along the direction perpendicular to the line joining the centers of the circular WG and bump. Since the true LHCP-like propagating modes in the chiral PhC slightly deviate from the guiding modes of the circular PEC WG, and the copper block is not infinitesimally small, a finite residual reflection is expected at ρ_s =0 even though the complete transparency is suggested by $g(\rho_s)$=0. Therefore, we approximate the realistic reflection coefficient $r(\omega)$ of the copper scatter in the form of $r(\omega)$~$ag(\rho_s)+b$ where a is a proportional factor; and b accounts for the residual reflection. The numerical data are then fitted with $|r(\omega)|^2$ based on this relation. As shown in Fig. 6, the fitting curve agrees well with the numerical data. The result also indicates that an arbitrary scatter, even if it is not chiral, also backscatters more efficiently as it is farther away from the center of the chiral PhC.

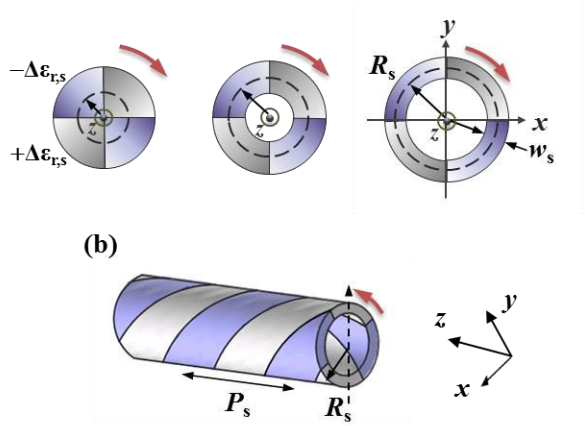

Figure 3. (a) Cross sections of 2-fold scatters as the radius R_s is varied. The cross-sectional areas are fixed at $0.3\pi R^2$. (b) The side view of a 2-fold left-handed scatter. The red arrow indicates handedness. P_s denotes the helical pitch.

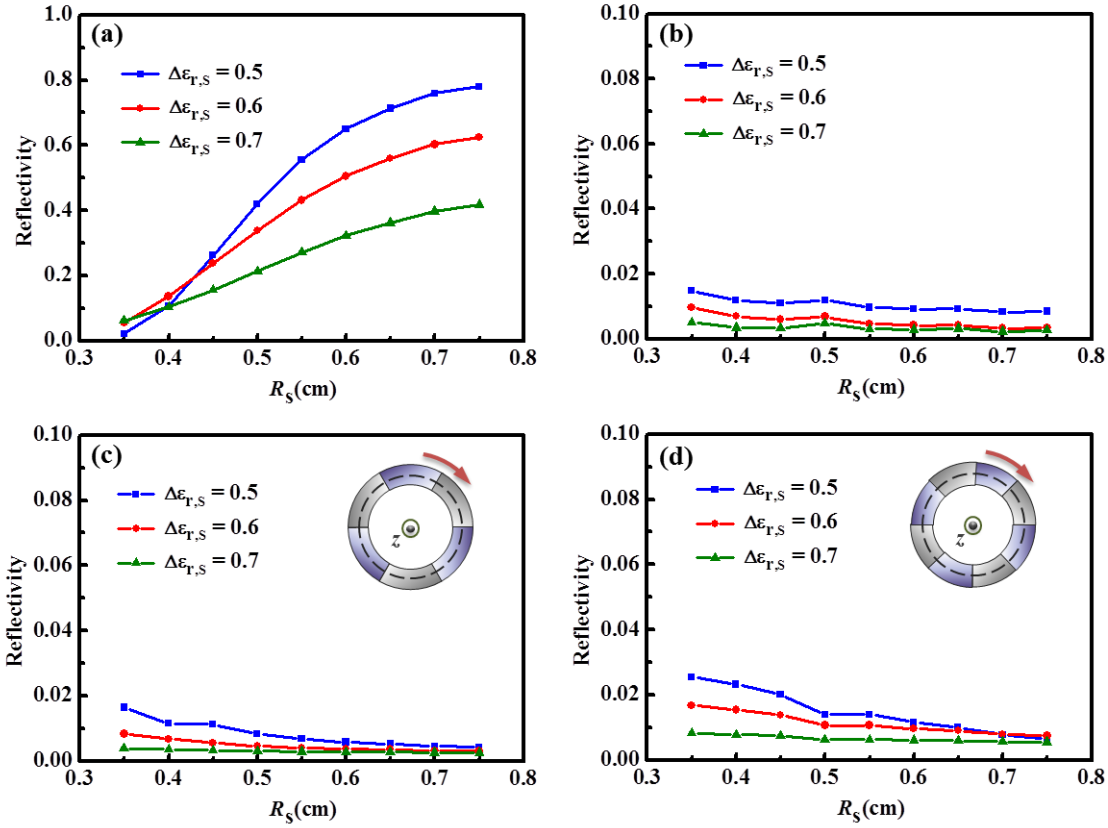

Figure 4. The reflectivities of the (a) 2-fold LH scatters, (b) 2-fold RH scatters, (c) 3-fold LH scatters and (d) 4-fold LH scatters as a function of R_s at various $\Delta\varepsilon_{r,s}$. Prominent backscattering takes place when the 2-fold LH scatters are present. Their RH counterparts show the much smaller reflectivities. Both 3-fold and 4-fold LH scatters do not backscatter significantly.

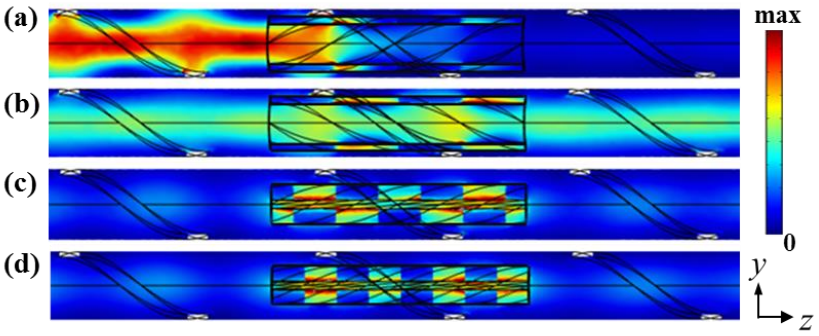

Figure 5. The field distributions on the *y*-*z* plane in the presence of (a) 2-fold LH scatters and (b) 2-fold RH scatters with R_S=0.7R at $\Delta\varepsilon_{r,s}$ =0.7, and the counterparts corresponding to (c) 3-fold LH scatters and (d) 4-fold LH scatters with R_s=0.3R at $\Delta\varepsilon_{r,s}$ =0.7. The incident field is hardly backscattered by the RH scatter. Except for the strong local fields around the scatters, the magnitudes of the propagating waves change little in these two cases.

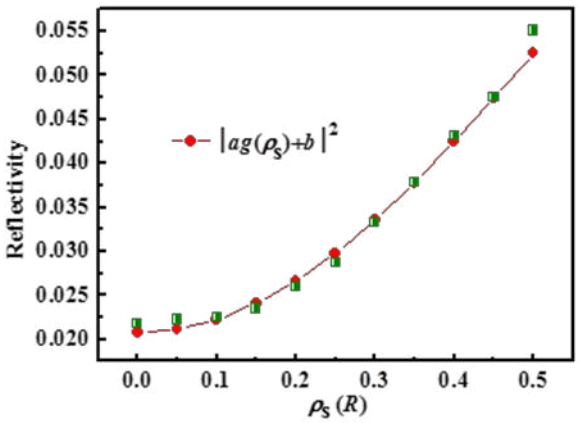

Figure 6. The reflectivity of a small copper block with a size of 0.3R × 0.5R × 0.5R versus the position ρ_s. The fitting curve shows a decent agreement with the numerical data.

5. CONCLUSIONS

While the propagation modes in a strongly-guided chiral one-way photonic crystal are immune to backscattering from many types of obstacles, they are, nevertheless, not really scattering-proof. We use the perturbative method to obtain the criteria for the prominent backscattering in such chiral structures. A few chiral/achiral scatters are numerically studied, and the trends of scattering agree well with our analytical approach. In absence of nonreciprocity, the scattered amplitude depends on the azimuthal Fourier components of scatter cross sections at order l=±2. Chiral scatters without these Fourier components would not reflect the chiral propagating modes efficiently. In addition, for these chiral photonic modes, the disturbance at the most intense point on the modal profile does not necessarily lead to the most efficient backscattering. These characteristics reveal what types of defects or scatters should be avoided in one-way applications of chiral structures in order to minimize the backscattering.

ACKNOWLEDGMENTS

This work is sponsored by Research Center for Applied Sciences, Academia Sinica, Taiwan and Ministry of Science and Technology, Taiwan under Grant numbers MOST-103-2221-E-001-016 and MOST-104-2221-E-001-018.

REFERENCES

[1] D. Jalas, A. Petrov, M. Eich, W. Freude, S. Fan, Z. Yu, R. Baets, M. Popovic, A. Melloni, J. D. Joannopoulos, M. Vanwolleghem, C. R. Doerr, and H. Renner, "What is–and what is not–an optical isolator," Nature Photon. 7, 579-582 (2013).

[2] K. v. Klitzing, G. Dorda, and M. Pepper, "New method for high-accuracy determination of the fine-structure constant based on quantized Hall resistance," Phys. Rev. Lett 45, 494-497 (1980).

[3] B. I. Halperin, "Quantized Hall conductance, current-carrying edge states, and the existence of extended states in a two-dimensional disordered potential," Phys. Rev. B 25, 2185–2190 (1982).

[4] X. G. Wen, "Gapless boundary excitations in the quantum Hall states and in the chiral spin states," Opt. Express 43, 11025–11036 (1991).

[5] F. D. M. Haldane and S. Raghu, "Possible realization of directional optical waveguides in photonic crystals with broken time-reversal symmetry," Phys. Rev. Lett 100, 013904 (2008).

[6] Z. Wang, Y. D. Chong, J. D. Joannopoulos, and M. Soljacic, "Reflection-free one-way edge modes in a gyromagnetic photonic crystal," Phys. Rev. Lett. 100, 013905 (2008)

[7] S. Raghu and F. D. M. Haldane, "Analogs of quantum-Hall-effect edge states in photonic crystals," Phys. Rev. A 78, 033834 (2008)

[8] Z. Wang, Y. Chong, J. D. Joannopoulos, and M. Soljacic, "Observation of unidirectional backscattering-immune topological electromagnetic states," Nature 461, 772–775 (2009)

[9] X. Ao, Z. Lin, and C. T. Chan, "One-way edge mode in a magneto-optical honeycomb photonic crystal," Phys. Rev. B 80, 033105 (2009).

[10] J.-X. Fu, R.-J. Liu, and Z.-Y. Li, "Robust one-way modes in gyromagnetic photonic crystal waveguides with different interfaces," Appl. Phys. Lett. 97, 041112 (2010)

[11] Y. Poo, R.-x. Wu, Z. Lin, Y. Yang, and C. T. Chan, "Experimental realization of self-guiding unidirectional electromagnetic edge states," Phys. Rev. Lett. 106, 093903 (2011)

[12] K. Fang, Z. Yu, and S. Fan, "Microscopic theory of photonic one-way edge mode," Phys. Rev. B 84, 075477 (2011)

[13] K. Fang, Z. Yu, and S. Fan, "Realizing effective magnetic field for photons by controlling the phase of dynamic modulation," Nat. Photonics 6, 782–787 (2012)

[14] K. Fang and S. Fan, "Controlling the flow of light using the inhomogeneous effective gauge field that emerges from dynamic modulation," Phys. Rev. Lett. 111, 203901 (2013).

[15] A. B. Khanikaev, S. H. Mousavi, W.-K. Tse, M. Kargarian, A. H. MacDonald, and G. Shvets, "Photonic topological insulators," Nat. Mater. 12, 233–239 (2013).

[16] O. Pankratov, S. Pakhomov, and B. Volkov, "Supersymmetry in heterojunctions: band-inverting contact on the basis of $Pb_{1-x}Sn_xTe$ and $Hg_{1-x}Cd_xTe$," Solid State Commun. 61, 93–96 (1987).

[17] B. A. Bernevig, T. L. Hughes, and S.-C. Zhang, "Quantum spin Hall effect and topological phase transition in HgTe quantum wells," Science 314, 1757–1761 (2006).

[18] H. Cory, "Chiral devices-an overview of canonical problems," J. Electromagnet Wave 9, 805–829 (1995).

[19] G. Shvets, "Optical polarizer/isolator based on a rectangular waveguide with helical grooves," Appl. Phys. Lett. 89, 141127 (2006).

[20] W.-J. Chen, Z. H. Hang, J.-W. Dong, X. Xiao, H.-Z. Wang, and C. T. Chan, "Observation of backscattering immune chiral electromagnetic modes without time reversal breaking," Phys. Rev. Lett. 107, 023901 (2011).

[21] COMSOL Multiphysics [http://www.comsol.com/]

[22] Pi-Ju Cheng, Chung-Hao Tien, and Shu-Wei Chang, "Incomplete immunity to backscattering in chiral one-way photonic crystals," Opt. Express 23, 10327-10340 (2015).